fishes

MDPI

Article

Effects of Simulated Tunnel Darkness on Histology of *Schizothorax macropogon*

Yanlin Wei [1,2], Hongze Li [3], Junjie Huang [1,2], Wei Liu [4], Jianguang Qin [5], Jianzhang Lv [3,*] and Tao He [1,2,*]

[1] College of Fisheries, Southwest University, Chongqing 400715, China
[2] Key Laboratory of Freshwater Fish Reproduction and Development (Ministry of Education), Key Laboratory of Aquatic Science of Chongqing, Chongqing 400715, China
[3] Hydraulic Engineering Department, Nanjing Hydraulic Research Institute, Nanjing 210029, China
[4] Jiacha Hydropower Plant, Huaneng Tibet Yarlung Zangbo River Hydropower Development & Investment Co., Ltd., Shannan 856400, China
[5] College of Science and Engineering, Flinders University, Adelaide 5001, Australia
* Correspondence: jzlv@nhri.cn (J.L.); hh1985@swu.edu.cn (T.H.)

Abstract

Schizothorax macropogon is an endemic fish species of the Tibetan Plateau whose distribution largely overlaps with hydropower facilities. In this study, the fish were exposed to simulated tunnel darkness for 7 days to evaluate microstructural changes in the gills, dorsal muscle, and midgut. The results showed that gill lamellae exhibited divergent trends with continued bending and shortening in the dark group, contrasting with rupture in the control group. Moreover, the number of mitochondria-rich cells in the dark group increased initially and then decreased, while remaining stable and evenly distributed in the control group. No significant pathological damage was observed in the skeletal muscles of both groups, and muscle fiber diameters displayed a "V"-shaped trend over time in both groups. However, muscle fiber diameters were significantly smaller in the dark group than in the control group. Furthermore, intestinal villus height decreased continuously over time in both groups, with goblet cell numbers initially rising before falling and consistently remaining lower in the dark group compared to the control group. These findings suggest that short-term exposure to darkness may disrupt circadian rhythms, induce behavioral anomalies and energy metabolism disorders, leading to microstructural alterations in gill, muscle, and intestinal tissues that reflect either adaptation or damage. This study provides histological insights into the physiological effects of tunnel darkness on fish and offers key scientific evidence for optimizing lighting conditions in plateau tunnel fishways.

Keywords: *Schizothorax macropogon*; simulated tunnel; darkness; histology

Key Contribution: This study provides the first histological assessment of the physiological impacts of simulated tunnel darkness on the gill, dorsal muscle, and midgut tissues of the endemic Tibetan Plateau fish, *Schizothorax macropogon*. The findings highlight significant microstructural alterations induced by dark stress, offering critical scientific evidence for optimizing lighting conditions in plateau tunnel fishways.

Check for updates

Academic Editor: Luisa María Vera

Received: 26 March 2026
Revised: 30 April 2026
Accepted: 5 May 2026
Published: 5 June 2026

Copyright: © 2026 by the authors. Licensee MDPI, Basel, Switzerland. This article is an open access article distributed under the terms and conditions of the Creative Commons Attribution (CC BY) license.

1. Introduction

To enhance the utilization and regulation of water resources, numerous hydraulic structures, including dams and weirs, have been built along major rivers in China. Although these projects have greatly promoted economic development, they have also caused

increasingly severe ecological problems [1]. For migratory fish species, the disruption of river connectivity caused by hydropower development makes fish passage facilities critical for migration [2,3]. Among these, fishways play a key role in restoring genetic exchange between upstream and downstream populations, thereby reducing the negative impacts of disrupted flow regimes and physical obstructions [4]. Tunnel-type fishways, a type of passage structure, are typically adapted from natural tunnels and offer advantages such as high feasibility and relatively low construction costs [5]. Compared to natural riverine environments, the light conditions within fishways associated with hydropower projects exhibit substantial variability in illumination, broad spectral ranges, and complex interactions with water flow. Specifically, in tunnel-type fishways, open-channel segments are generally shallow and exposed to natural light, while tunnel segments remain in complete darkness, resulting in pronounced differences in light intensity between the two sections [6]. In recent years, some scholars have conducted research on the influence of the dark environment in tunnels on the upstream behavior of fish. It was reported that dark tunnel environments delayed fish migration and reduced passage efficiency [6]. Additionally, the influence of light conditions on fish behavioral responses has attracted growing attention [7]. It was observed that *Schizothorax prenanti* exhibited positive phototactic behavior toward the blue and green light under hydrostatic and hydrodynamic conditions, but negative phototactic behavior toward red and yellow light, showing a preference for low luminance intensities, and its phototactic behavior did not increase with rising water flow rates [8]. Similarly, it was demonstrated that zebrafish displayed differential phototactic responses to various wavelengths, with a higher preference for red, green, and purple light, but a lower preference for yellow light [9]. This further underscores the pivotal role of the light environment in shaping fish behavior.

Schizothorax macropogon (Figure 1), known locally as "Huzi fish", is a species in the family Cyprinidae, order Cypriniformes, and is listed as a national class II protected animal in China [10]. Endemic to the Tibetan Plateau, this fish primarily inhabits the Yarlung Zangbo River and its tributaries. As an endemic dominant species in this region, *S. macropogon* maintains high population abundance and occupies a critical ecological niche within the riverine ecosystem [11,12]. Its distribution exhibits substantial spatial overlap with the plateau hydropower infrastructure [13], thereby rendering it a species of significant importance for watershed biodiversity and river ecological connectivity.

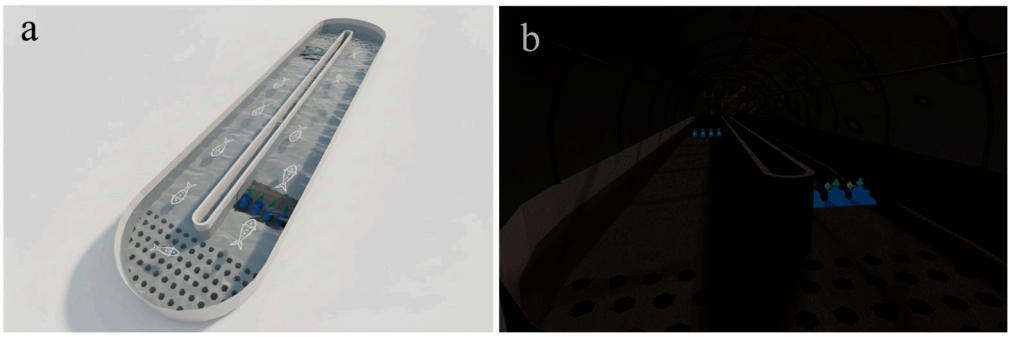

Figure 1. Schematic diagram of the experimental setup. (**a**) the flume under simulated natural light conditions; (**b**) the flume under simulated dark conditions.

Schizothoracine fishes have evolved distinctive molecular and morphological adaptations in response to extremely high-altitude environments characterized by hypoxia, low temperatures, and rapid flows [14]. Genomic studies reveal a genetic foundation for high-altitude adaptation in this subfamily. For example, *Gymnodiptychus pachycheilus* shows genome-wide accelerated evolution in genes related to energy metabolism and hypoxia response [15], while genomic analysis of *Schizopygopsis younghusbandi* has identified

significant expansions in gene families involved in energy storage and metabolism, as well as positively selected genes associated with oxygen transport and energy regulation, collectively enhancing adaptation to cold and hypoxic conditions [16]. Morphologically, these fishes possess specialized oral structures, well-developed barbels, and modified gill rakers and arches that support feeding and respiration in fast-flowing, oxygen-deficient waters [14]. Furthermore, tissues such as the gills and intestine exhibit considerable plasticity under stressors like hypoxia and strong currents, adapting through changes in lamellar morphology, epithelial thickness, and intestinal goblet cell abundance [17].

Although these studies have elucidated multiple aspects of the adaptive mechanisms of schizothoracine fishes, the effect of tunnel darkness, an artificial environment from hydropower development, on the tissue architecture of *S. macropogon* remains unknown. Considering that the gill is the primary interface for gas exchange, osmoregulation, and nitrogen waste excretion, and its structural integrity is essential for respiratory efficiency and internal homeostasis [18]. Muscle tissue is the key organ enabling migration and upstream movement in fishes and also serves as an important reservoir of protein and energy, directly reflecting metabolic status and locomotor capacity [9]. And the intestine, as the central site for nutrient absorption and mucosal immune defense, plays a vital role in evaluating the nutritional status and overall health of the organism [19]. In this study, gills, dorsal muscle, and midgut tissues were selected as representative organs to investigate the histological responses of *S. macropogon* to a simulated 7-day tunnel-darkness model. By comparing the microstructural alterations of these tissues under natural light and complete darkness, this study aims to systematically assess the potential tissue-level damage induced by dark stress, thereby providing histological evidence for optimizing light environments and ecological protection strategies in plateau fishway tunnels.

2. Material and Method

2.1. Experimental Materials

A total of 100 healthy adult *S. macropogon* were purchased from a commercial aquaculture farm in Nyingchi, Tibet, China. The selected fish were uniform in size, exhibited normal coloration, were in good health without any external injuries, and the mean body weight (BW) was 561.45 ± 132.42 g, and the mean total length (TL) was 39.63 ± 2.73 cm. Prior to the experiment, the fish were acclimated for 7 days in a 3 m^3 circular tank supplied with flowing water. During acclimation, water quality remained at DO ≥ 7.5 mg L^{-1}, pH 7.5 ± 0.5, TAN < 0.1 mg L^{-1}, and NO_2^- < 0.01 mg L^{-1} under a 12L:12D photoperiod. The experiment utilized two identical recirculating flumes (16 m × 3.5 m × 1 m) operating at the design velocity of the prototype tunnel fishway. The control (L group) was exposed to natural light (Figure 1a), whereas the experimental group (D group) was housed in a closed, dark flume simulating a tunnel environment (Figure 1b). Both were stocked concurrently with test fish. A steady flow was maintained by four variable-frequency pumps, with water drawn from the surface layer through perforated inlet plates and returned via an outlet ramp.

2.2. Experimental Design

Before the experiment, the two recirculating flumes were hydraulically standardized to identical flow regimes. The experiment was conducted using two identical recirculating flumes, with one flume assigned to the L group and the other to the D group. A total of 100 fish were randomly distributed between the two flumes. No food was provided throughout the experiment to simulate natural fasting during fishway passage. Daily 33% water exchanges were conducted to maintain DO > 7.5 mg L^{-1}, pH 7.5 ± 0.5, TAN < 0.1 mg L^{-1}, and NO_2^- < 0.01 mg L^{-1}. All experimental procedures involving ani-

mals were approved by the Institutional Animal Care and Use Committee of Southwest University (IACUC-20260317-09; Approval Date: 18 March 2026). On days 1, 2, 3, and 7 of the experiment, nine fish per flume were randomly collected, euthanized with MS-222, and measured for TL, SL, and BW. The specific data are presented in Supplementary Table S1.

2.3. Tissue Processing

Subsequently, the gill, dorsal muscle and midgut samples were collected, rinsed three times with precooled 0.9% NaCl solution (4 °C) and then fixed in 4% paraformaldehyde (1:10 *w*/*v*). including graded ethanol dehydration, paraffin embedding, and sectioning at approximately 3 μm using a rotary microtome (Leica RM2016, Nussloch, Germany), with minor adjustments within 2–5 μm for a few samples according to sectioning quality. The sections were then deparaffinized, stained with hematoxylin–eosin (H&E), and mounted with neutral balsam. A relatively thin section thickness was adopted because thicker sections were more prone to detachment during staining and did not provide satisfactory section quality for subsequent microscopic observation. Microscopic observations and image acquisition were performed using an Olympus CX33 light microscope (Olympus, Tokyo, Japan) with 4× and 10× objective lenses. Subsequently, the histological sections were scanned using a Pannoramic 250 digital slide scanner (3DHISTECH, Budapest, Hungary), which was used for image acquisition and measurement of the width and length of gill lamellae, interlamellar distance, muscle fiber diameter, muscle fiber count (N/100 ×), muscular layer thickness, villus height, and goblet cell count (N/100 ×).

2.4. Semi-Quantitative Histopathological Assessment

To complement the descriptive histological observations, tissue lesions were further summarized using a semi-quantitative grading approach [20–23]. Based on the dominant pathological alterations observed in histological sections at each sampling time point, an overall lesion grade was assigned for the gills, dorsal muscle, and midgut. Lesion severity was graded on a five-point scale as follows: 0, no detectable lesion; 1, slight lesion; 2, mild lesion; 3, moderate lesion; and 4, severe lesion. The grading was determined according to the extent and severity of the major histopathological alterations observed in each organ, including structural disruption, degenerative changes, and inflammatory responses. This grading system was used to support the descriptive histological observations and to provide a more structured comparison of lesion severity among groups and sampling time points.

2.5. Statistical Analysis

Data were presented as the mean ± SD. Prior to statistical analyses, data were tested for normality using the Shapiro–Wilk test and for homogeneity of variances using Levene's test. One-way ANOVA was performed using SPSS 27.0 (IBM Corp., Armonk, NY, USA). Duncan's multiple range test was used for intragroup comparisons, and T-tests were employed for intergroup comparisons. A value of $p < 0.05$ was considered to indicate a significant difference, while $p < 0.01$ was considered to indicate an extremely significant difference.

3. Result

3.1. Effects of Simulated Tunnel Darkness on the Structure of Gill in S. macropogon

The gills of *S. macropogon* are composed of gill arches bearing gill filaments, with gill rakers located on the inner margin of the arches. Each gill filament contains a central cartilaginous axis and supports numerous comb-like, arranged lamellae on both sides (Figure 2I). Its distal end forms a unique club-shaped swelling, devoid of lamellae but rich

in chondrocytes and goblet cells (Figure 2II). The respiratory lamellae contain flattened pavement cells, pillar cells forming and support the blood channels for gas exchange, and mucus-secreting goblet cells for protection (Figure 2III). Gill arches anchor the filaments and support serrated rakers on their inner margins. These rakers are primarily composed of epithelial and connective tissues, populated by tightly packed epithelial cells and larger, sparsely distributed, cup-shaped goblet cells (Figure 2IV).

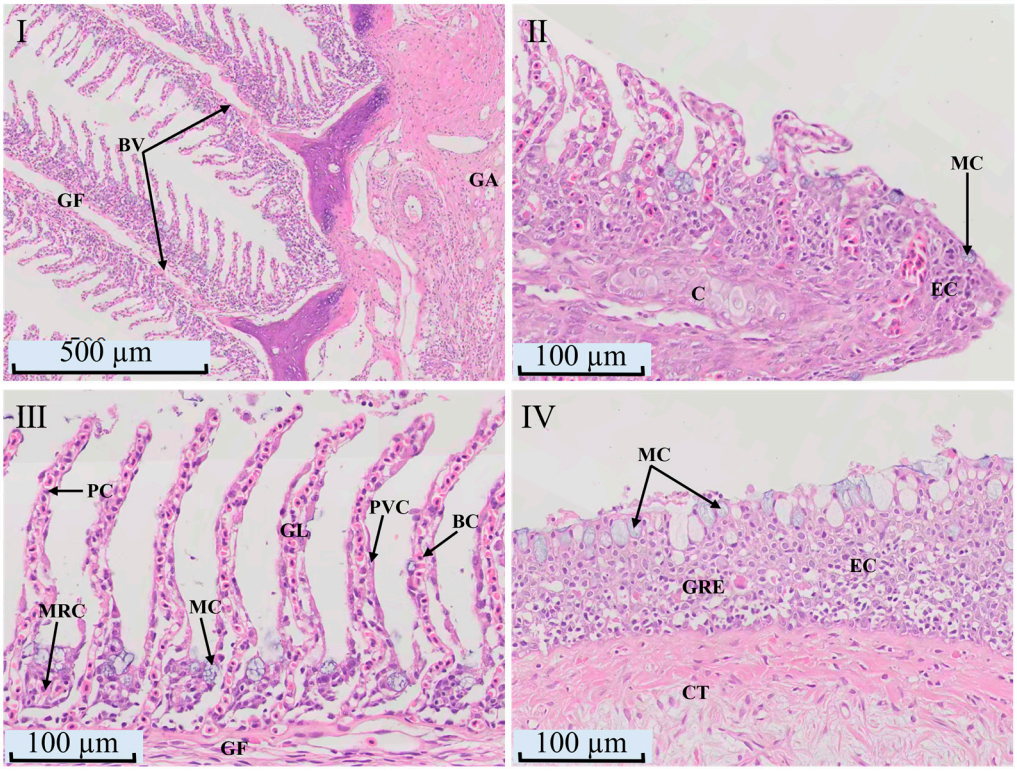

Figure 2. The light micrographs of normal gill tissue in *S. macropogon*. (**I**) Gill filaments and arch (4×); (**II**) Apex of gill filament (20×); (**III**) Gill lamellae (20×); (**IV**) Gill rakers (20×). GF: gill filament; GA: gill arch; GL: gill lamella; BV: blood vessel; MC: mucous cell; EC: epithelial cell; C: chondrocyte; GRE: gill raker epithelium; CT: connective tissue; PC: pillar cell; MRC: mitochondria-rich cell; PVC: pavement cell; BC: blood cell.

Histological sections showed time-dependent morphological changes in gill lamellae in both groups (Figure 3). In the L group, the number of MRCs (mitochondria-rich cells) remained stable, but blood sinus space increased, and swelling occurred at the lamellar ends by L2. By L3, these changes became more pronounced, with epithelial detachment and bending at tips. By L7, severe bending and rupture due to blood cell accumulation and epithelial loss were observed. In the D group, pathological changes appeared earlier and were more severe, with increased MRCs and generalized bending by D2. By D7, lamellar bending progressed, but MRCs decreased.

Measurement results revealed distinct changes in gill lamellae. Lamellar width peaked on D3 and declined by D7, with the D group generally wider than the L group. Lamellar length showed a "V"-shaped response to light but shortened progressively in darkness. Interlamellar distance shortened on D2 and lengthened on D3 in both groups, but by D7, it continued to lengthen in the D group while shortening in the L group (Table 1).

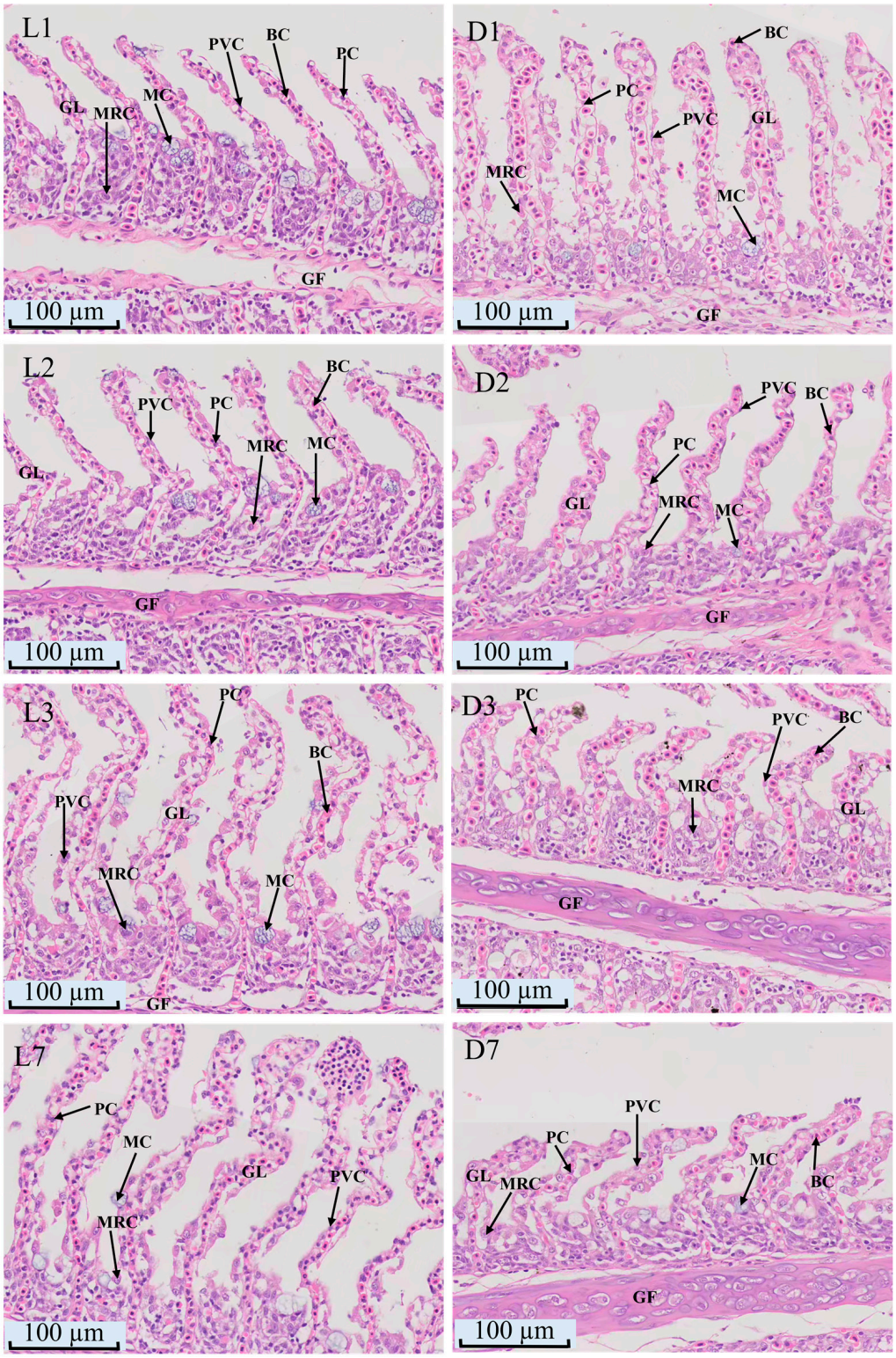

Figure 3. Light micrographs of gill lamellae in *S. macropogon* exposed to L group or D group (20×). L1, L2, L3, L7: gill lamellae from the L group on days 1, 2, 3, and 7, respectively; D1, D2, D3, D7: gill lamellae from the D group on days 1, 2, 3, and 7, respectively; GF, gill filament; GL, gill lamella; PC, pillar cell; PVC, pavement cell; MC, mucous cell; MRC, mitochondria-rich cell; BC, blood cell.

Table 1. Effects of L group versus D group on the gill lamella of *S. macropogon*.

Index	Groups	Times			
		1	2	3	7
The width of gill lamella (μm)	L	15.84 ± 3.18 ^{d}	16.65 ± 2.40 ^{d}	35.36 + 4.28 ^{a}	22.77 + 7.08 ^{c}
	D	24.52 ± 3.57 ^{c}	31.79 ± 4.68 ^{ab}	31.97 ± 4.68 ^{ab}	28.64 + 3.90 ^{b}
The length of secondary gill lamella (μm)	L	185.61 ± 10.69 ^{de}	177.21 ± 6.58 ^{e}	283.27 ± 15.03 ^{b}	299.00 ± 27.57 ^{a}
	D	234.39 ± 8.21 ^{c}	192.46 ± 9.54 ^{d}	136.63 ± 5.12 ^{f}	135.58 + 10.92 ^{f}
The intervals of secondary gill lamella (μm)	L	45.22 + 3.52 ^{b}	45.10 + 5.13 ^{b}	55.80 + 2.85 ^{a}	37.36 ± 4.74 ^{c}
	D	37.50 + 2.81 ^{c}	31.98 ± 3.96 ^{d}	35.13 ± 6.23 ^{cd}	48.83 ± 7.18 ^{b}

Note: Data are presented as mean ± SD (n = 9). Under the same index, values with different superscript letters indicate significant differences between groups ($p < 0.05$).

3.2. Effects of Simulated Tunnel Darkness on the Structure of Dorsal Muscle in S. macropogon

The dorsal muscle of *S. macropogon* is primarily composed of three layers of connective tissue structures: the epimysium, perimysium, and endomysium, which sequentially encase the muscle fiber bundles and muscle fibers in a hierarchical arrangement (Figure 4). At low magnification (4×), the relatively thick epimysium can be observed, enveloping the entire muscle tissue and forming a complete external structural outline (Figure 4 I). At medium magnification (20×), the perimysium distinctly demarcates the muscle fiber bundles into multiple functional units (Figure 4 II), with the bundles closely packed together, resulting in a dense and well-organized overall structure. At high magnification (80×), each muscle fiber is seen to be encased by the endomysium (Figure 4 III). The endomysium, a fine connective tissue layer, closely adheres to the sarcolemma of the muscle fiber. In transverse sections of muscle fibers, the nuclei can be clearly identified as being attached beneath the sarcolemma, while the cytoplasm appears homogeneous with numerous filamentous structures dispersed within, which are the myofibrils.

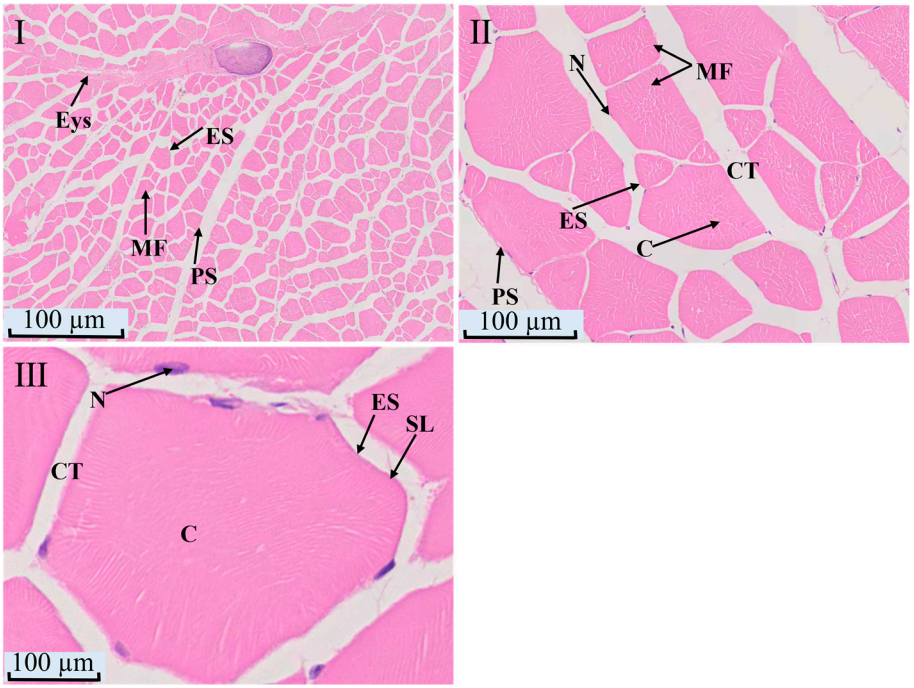

Figure 4. The light micrographs of normal dorsal muscle tissue in *S. macropogon*. (**I**) Epimysium (Eys) surrounding the muscle fiber bundles (4×); (**II**) Perimysium (PS) surrounding the muscle fiber bundles (20×); (**III**) Endomysium (ES) surrounding individual muscle fibers (80×); Eys: epimysium; PS: perimysium; ES: endomysium; SL: sarcolemma; MF: muscle fiber; C: sarcoplasm; N: myocardial nucleus; CT: connective tissue; M: myofibril.

Histological observations (Figure 5) revealed that the muscle tissues of both the L group and the D group remained relatively intact throughout the experimental period. The muscle fibers in both groups were arranged in an orderly manner, with clear and well-defined muscle fascicle structures. The muscle fiber morphology was regular, with nuclei located beneath the muscle membrane, and the myofibrils were clearly visible and intact.

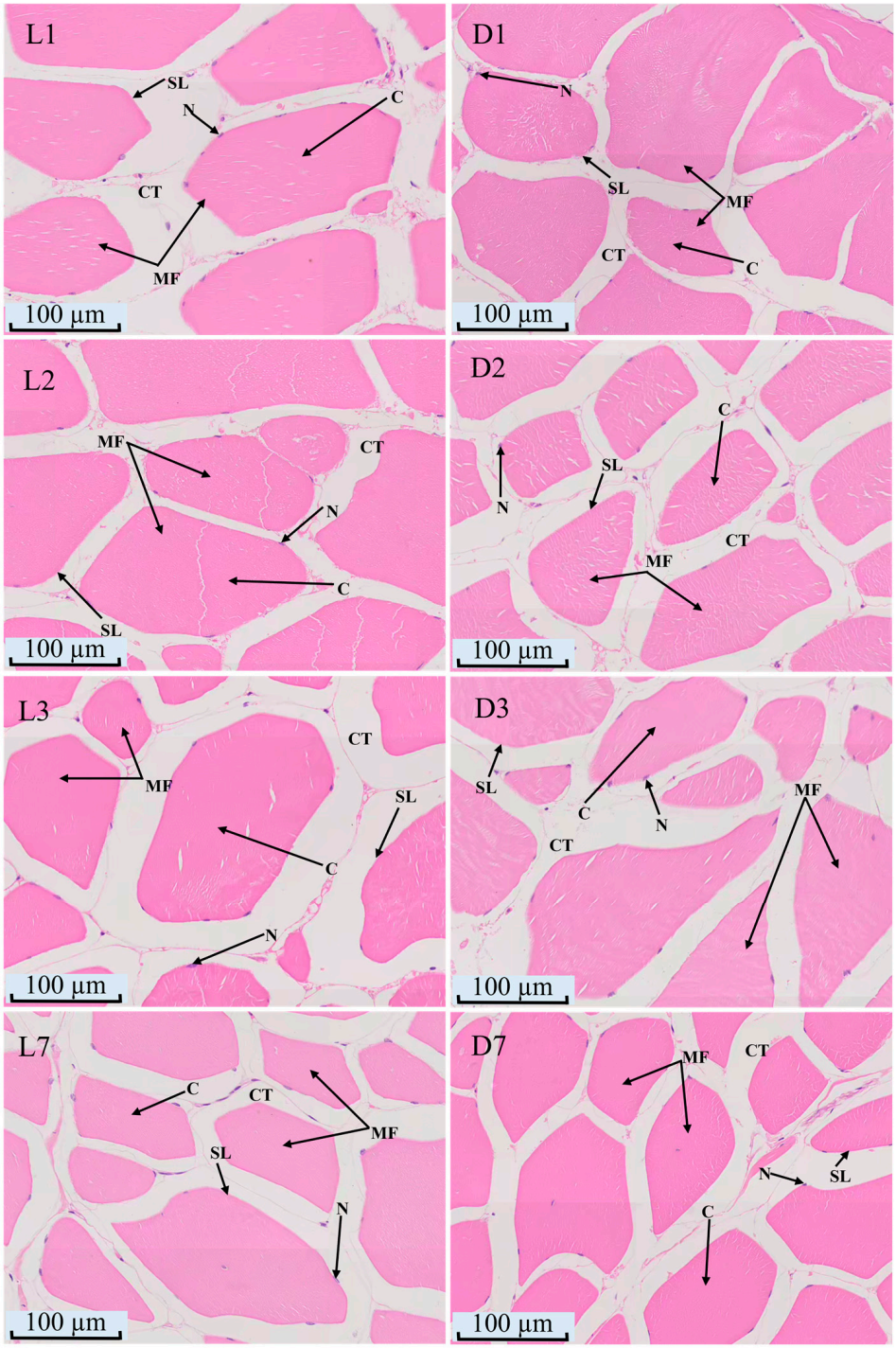

Figure 5. Light micrographs of dorsal muscle in *S. macropogon* exposed to L group or D group (20×). L1, L2, L3, L7: dorsal muscle from the L group on days 1, 2, 3, and 7, respectively; D1, D2, D3, D7: dorsal muscle from the D group on days 1, 2, 3, and 7, respectively; C: sarcoplasm; N: myocardial nucleus; CT: connective tissue; SL: sarcolemma; MF: muscle fiber.

The measurement data (Table 2) showed that the muscle fiber diameter in both the L group and the D group exhibited a "V"-shaped trend, with the lowest value observed on day 3 and a subsequent increase by D7. The muscle fiber diameter in the L group was significantly larger than that in the D group at all time points ($p < 0.05$). In terms of muscle fiber number, both groups exhibited an inverted "V"- shaped trend, with the D group having a higher number of muscle fibers than the L group at all time points, and the maximum number of muscle fibers was reached on day 3.

Table 2. Effects of L group versus D group on the dorsal muscle of *S. macropogon*.

Index	Groups	Times			
		1	2	3	7
The muscle fiber diameter (μm)	L	126.08 + 13.49 ^{a}	112.91 + 25.76 ^{ab}	98.56 ± 22.68 ^{bc}	122.83 + 13.62 ^{a}
	D	98.13 + 17.28 ^{bc}	92.26 ± 16.55 ^{cd}	78.28 ± 21.22 ^{d}	91.09 ± 10.19 ^{cd}
The muscle fiber number (N/100×)	L	48.00 + 16.82 ^{b}	75.33 + 15.18 ^{ab}	97.33 ± 10.69 ^{ab}	65.67 ± 12.58 ^{ab}
	D	98.00 + 13.00 ^{ab}	126.67 ± 75.64 ^{ab}	136.67 ± 64.42 ^{a}	107.33 ± 4.04 ^{ab}

Note: Data are presented as mean ± SD ($n = 9$). Under the same index, values with different superscript letters indicate significant differences between groups ($p < 0.05$).

3.3. Effects of Simulated Tunnel Darkness on the Structure of Midgut in S. macropogon

Histological sections show that the intestinal mucosa of *S. macropogon* folds inward to form finger-like villi. The intestinal wall comprises four orderly layers, the mucosa, submucosa, muscularis and serosa (Figure 6I). From the inner lumen to the outer surface, the intestinal wall comprises four orderly layers, the mucosa, submucosa, muscularis and serosa (Figure 6II,III). Lymphocytes are interspersed among the epithelial cells (Figure 6III). The lamina propria and submucosa are both connective tissues rich in blood vessels (Figure 6II–IV). The muscularis has a more developed inner circular layer and a thinner outer longitudinal layer, with nerve cells between them. The serosa is a thin layer of connective tissue covered by mesothelium (Figure 6V).

Histological sections show significant morphological changes in intestinal tissue over time in both the L and D groups (Figure 7). In the L group, no changes were observed from L1 to L2, but by L3, the submucosa thickened and villi shortened. By L7, villi showed further reduction in height and disordered arrangement. The D group exhibited more pronounced changes. At D2, goblet cells increased and submucosa thickened, but by D3, the submucosa thinned. By D7, villi were shorter, and goblet cells decreased significantly. Throughout the experiment, the L group had fewer goblet cells than the D group.

Measurements indicate that in the L group, muscular layer thickness initially increased then decreased, with significant differences at L2 compared to L1 ($p < 0.05$), and at L3 and L7 compared to L1 and L2 ($p < 0.05$). Villus height decreased continuously, with significant reductions at L3 and L7 ($p < 0.05$). Goblet cell numbers increased significantly at L3 ($p < 0.05$) but remained stable otherwise. In the D group, muscular layer thickness fluctuated, increasing at D2, decreasing at D3, and rising again at D7 ($p < 0.05$). Villus height decreased continuously, reaching the lowest point at D7 ($p < 0.05$). Goblet cell numbers showed an inverted "V"-shaped change, peaking at D2 and dropping to the lowest level at D7, remaining significantly lower than the L group throughout (Table 3).

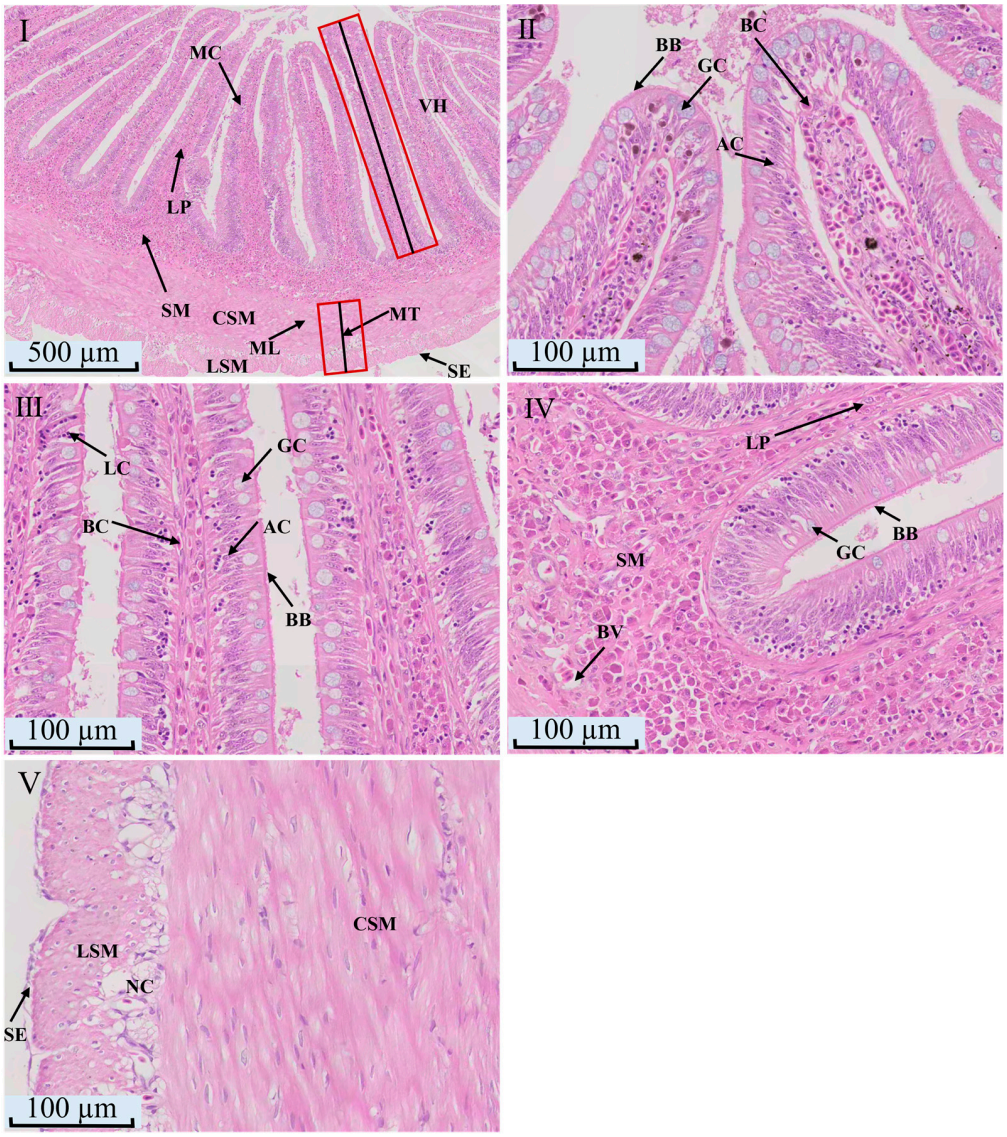

Figure 6. The light micrographs of midgut tissue in *S. macropogon.* (**I**) overview of normal intestinal sections (4×); (**II**) apical mucosa (20×); (**III**) mid-mucosal region (20×); (**IV**) submucosa (20×); (**V**) muscular layer (20×). In panel (**I**), the two red outlined boxes and their black middle lines indicate the complete regions of villus height and muscular layer thickness, respectively. VH: villus height; MT: muscular layer thickness; SE: serous membrane; ML: muscular layer; SM: submucous layer; MC: mucous layer; LSM: longitudinal smooth muscle; CSM: circular smooth muscle; BV: blood vessels; GC: goblet cells; BB: brush border; AC: absorptive cells; BC: blood cells; LC: lymphocytes; NC: neurons.

3.4. Semi-Quantitative Histopathological Assessment of Tissue Lesions

To complement the descriptive histological observations, tissue lesions in the gills, dorsal muscle, and midgut were further summarized using a semi-quantitative grading approach (Table 4). In the gills, lesion severity increased progressively over time in both groups, whereas the D group showed earlier onset and greater severity than the L group. The gill lesion grade in the L group increased from 1 on day 1 to 4 on day 7, whereas the D group increased more rapidly, reaching grade 3 on day 2 and grade 4 on days 3 and 7. In dorsal muscle, the lesion grade remained 0 throughout the experiment in both groups, indicating that no obvious histopathological abnormality was observed. These findings were consistent with the descriptive histological observations showing orderly fiber arrangement and generally intact muscle structure. In the midgut, lesion severity also

increased over time in both groups, with the D group showing more pronounced changes than the L group. The L group remained at grade 0 on days 1 and 2, but increased to grades 2 and 3 on days 3 and 7, respectively. In contrast, the D group showed a progressive increase from grade 1 on day 1 to grade 4 on day 7. Overall, the semi-quantitative grading results were consistent with the descriptive histological observations and the corresponding morphometric measurements.

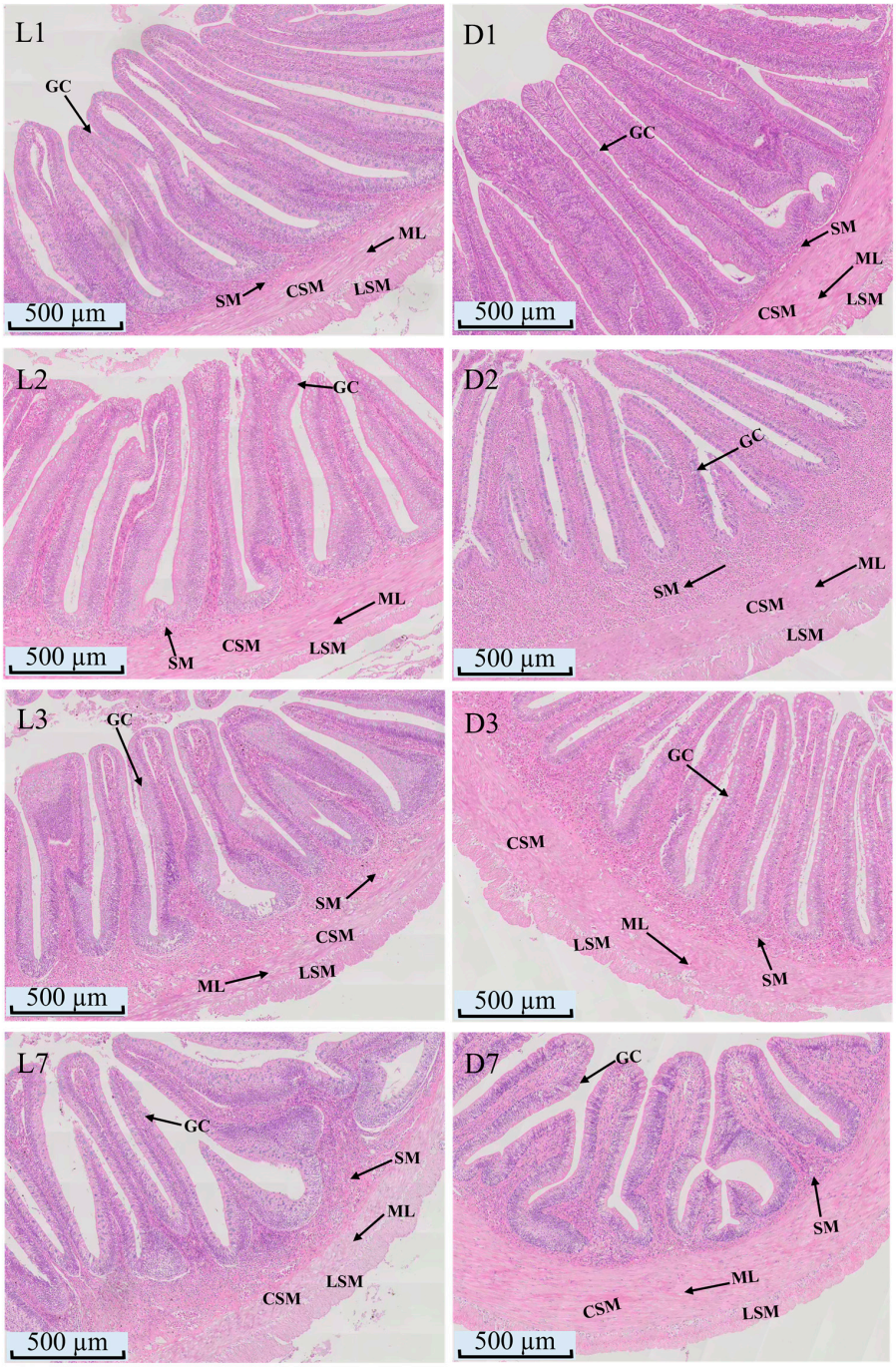

Figure 7. Light micrographs of midgut in *S. macropogon* exposed to L group or D group (4×). L1, L2, L3, L7: midgut from the L group on days 1, 2, 3, and 7, respectively; D1, D2, D3, D7: midgut from the D group on days 1, 2, 3, and 7, respectively; ML: muscular layer; SM: submucous layer; LSM: longitudinal smooth muscle; CSM: circular smooth muscle; GC: goblet cells.

Table 3. Effects of L group versus D group on the midgut of *S. macropogon*.

Index	Groups	Times			
		1	2	3	7
The muscular layer thickness (μm)	L	298.35 + 20.27 ^{c}	365.22 + 37.37 ^{a}	212.30 + 35.62 ^{d}	222.15 ± 23.80 ^{d}
	D	312.78 ± 21.28 ^{bc}	392.57 ± 20.60 ^{a}	233.89 ± 37.29 ^{d}	336.02 ± 31.91 ^{b}
The villus height (μm)	L	1370.00 + 111.92 ^{a}	1218.67 + 157.25 ^{b}	1163.32 + 171.34 ^{b}	944.21 ± 39.63 ^{c}
	D	1474.44 ± 92.48 ^{a}	1380.00 ± 99.87 ^{a}	945.21 ± 66.95 ^{c}	621.67 + 84.34 ^{d}
The goblet cell number (N/100×)	L	110.22 ± 17.07 ^{b}	101.22 + 18.12 ^{b}	184.78 + 24.11 ^{a}	104.11 ± 22.46 ^{b}
	D	60.33 ± 13.77 ^{a}	99.78 ± 17.93 ^{b}	94.22 ± 13.54 ^{b}	32.22 ± 7.22 ^{d}

Note: Data are presented as mean ± SD (n = 9). Under the same index, values with different superscript letters indicate significant differences between groups ($p < 0.05$).

Table 4. Semi-quantitative histopathological lesion grades in the gills, dorsal muscle, and midgut of *S. macropogon*.

Organ	Groups	Times			
		1	2	3	7
Gills	L	1	2	3	4
	D	1	3	4	4
Dorsal muscle	L	0	0	0	0
	D	0	0	0	0
Midgut	L	0	0	2	3
	D	1	2	3	4

Note: Lesion severity was graded on a five-point scale as follows: 0, no detectable lesion; 1, slight lesion; 2, mild lesion; 3, moderate lesion; and 4, severe lesion. The overall lesion grade at each sampling time point was assigned according to the dominant histopathological alterations observed in histological sections.

4. Discussion

4.1. Effects of Simulated Tunnel Darkness on the Structure of Gill in S. macropogon

The gills of *S.macropogon* primarily consist of gill filaments, gill arches, and gill rakers, similar to most teleost fishes [24]. The comb-like arrangement of gill lamellae and the structural characteristics of the gill blood sinuses reflect the efficient gas exchange [18]. Notably, the terminal end of each gill filament displays a rod-shaped structure rich in chondrocytes and mucous cells, lacking lamellae, which may provide mechanical support and mucus secretion, adapting to turbulent, high-altitude streams [25].

The gill epithelium mainly consists of filament and lamellar epithelium, where gas exchange occurs in the lamellar epithelium [26]. The distribution of pavement cells, pillar cells, and blood cells aligns with typical gas exchange and osmoregulation structures in fish. The regularly arranged pillar cells are crucial for maintaining the stability of the gill blood sinuses, similar to their role reported in zebrafish [27]. Mucous cells on the lamellae maintain gill surface moisture and prevent pathogen adhesion [24]. The gill rakers on the inner side of the gill arch are serrated, composed of epithelial and connective tissues, and may be related to filtering functions [28]. The epithelium contains many large, loosely arranged mucous cells, which may help in food particle adhesion, improving feeding efficiency [25].

Fish gill tissues are highly sensitive to environmental changes. According to our observations, under simulated tunnel fishway conditions with continuous water flow, both the L and D groups showed significant morphological changes in gill lamellae, including increased blood sinus space, lamellar swelling, and epithelial shedding, consistent with previous studies [18]. However, the D group exhibited more severe tissue damage, likely due to circadian disruption in the dark environment, affecting swimming behavior and increasing upstream migration frequency, thus exacerbating mechanical stress on the gills [6]. MRCs play a crucial role in osmoregulation [29]. In this study, the number of MRCs in the D group initially increased and then decreased. This dynamic response likely reflects a phased reaction

to combined darkness and hydrodynamic stress. Initially, increased upstream migration frequency due to circadian disruption led to more mechanical impact on gill lamellae, prompting fish to upregulate MRCs to compensate for ion loss [30]. However, sustained stress increased oxidative stress and energy expenditure, leading to a downregulation of MRCs to reduce maintenance costs and restore stability [31,32]. These histological changes were also supported by the semi-quantitative grading results, which showed that gill lesions developed earlier and were more severe in the D group than in the L group.

4.2. Effects of Simulated Tunnel Darkness on the Structure of Dorsal Muscle in S. macropogon

Microstructural observations reveal that the dorsal muscle tissue of *S. macropogon* is enveloped by three layers of connective tissue: the epimysium, perimysium, and endomysium, exhibiting typical characteristics of fish skeletal muscle [33]. The thick, continuous epimysium maintains the muscle's structural integrity and tensile strength, enabling the robust swimming performance demanded by flowing water habitats [34,35]. The perimysium compartmentalizes muscle fibers into functional units containing microvessels and nerve endings, facilitating metabolic support and efficient transmission of mechanical stress [36]. Each muscle fiber is closely enveloped by the endomysium, which supports structural stability and force distribution during contraction [35].

Fish skeletal muscle grows through coordinated remodeling of connective tissue and neural components [9]. Although no obvious pathological damage was observed, significant differences in muscle fiber diameter and number between groups indicated dynamic effects of behavioral rhythms and energy metabolism on muscle structure. In the L group, muscle fiber diameter showed a "V-shaped" trend, decreasing initially and recovering by day 7, remaining significantly larger than in the D group ($p < 0.05$). The initial reduction likely reflected increased energy expenditure from swimming activity, while the recovery suggested metabolic adaptations to reduce energy consumption and maintain protein balance [37,38]. However, slower recovery relative to initial reduction may be attributed to suppressed protein synthesis during fasting [39]. In contrast, the D group exhibited consistently smaller fiber diameters, indicating impaired muscle stability [40]. Dark-induced disruption of photoperiod perception and abnormal swimming behavior, combined with nutritional deprivation, likely promoted mitochondrial dysfunction, oxidative stress, and activation of proteolytic pathways such as the ubiquitin-proteasome system, collectively contributing to muscle atrophy [41]. The transient diameter increase on day 7 may result from a metabolic shift toward anaerobic pathways under prolonged fasting, leading to lactic acid accumulation, elevated osmotic pressure, and subsequent water influx into muscle fibers [42]. Muscle fiber number in both groups followed an "inverted V-shaped" trend without significant intergroup differences. The consistently higher fiber count in the D group may be partly attributable to reduced fiber diameter increasing visible fiber density per field, while greater individual variability suggests possible activation of compensatory hyperplastic mechanisms [43,44]. The L group demonstrated more stable fiber number regulation, reflecting maintained structural homeostasis under entrained circadian rhythms. This interpretation was consistent with the semi-quantitative grading results, in which dorsal muscle lesions remained at grade 0 in both groups throughout the experiment.

4.3. Effects of Simulated Tunnel Darkness on the Structure of Midgut in S. macropogon

Microstructural observations reveal that the intestinal wall of *S. macropogon* consists of the mucosa, submucosa, muscularis, and serosa, displaying the typical layered architecture of vertebrate intestines [45,46]. The mucosa forms finger-like villi that significantly increase the absorptive surface area, thereby enhancing nutrient absorption efficiency [47]. This layer is composed of a single layer of columnar epithelial cells with a well-developed

striated border, which is crucial for nutrient uptake [48]. Goblet cells, scattered among the epithelial cells, secrete mucus that lubricates the intestinal lumen and prevents pathogen adhesion, playing a vital role in mucosal immunity [49]. The presence of lymphocytes within the epithelium suggests active gut-associated lymphoid tissue (GALT), supporting local immune defense [50]. The muscularis, comprising inner circular and outer longitudinal muscle layers, indicates strong peristaltic capacity, facilitating the propulsion and mixing of intestinal contents [51]. The outer serosal layer provides structural support and protects against mechanical friction [52].

Under simulated tunnel conditions involving darkness and fasting, *S. macropogon* exhibited significant temporal changes in intestinal histoarchitecture, indicating that darkness disrupts morphological homeostasis. The initial increase in muscularis thickness in both L and D groups at day 2 may represent a short-term compensatory response to fasting [19]. However, the secondary increase observed in the D group at day 7, compared to L7, likely reflects circadian rhythm disruption under continuous darkness, leading to elevated energy demands and intestinal motility [53]. A notable reduction in villus height was observed, which directly diminishes the intestinal absorptive surface area and efficiency [54]. Furthermore, goblet cell abundance was consistently higher in the L group than in the D group, suggesting that dark exposure impairs intestinal barrier maintenance and compromises mucosal immune function [55]. These findings were further supported by the semi-quantitative grading results, which showed a progressive increase in intestinal lesion severity over time, with consistently higher grades in the D group than in the L group.

In addition to descriptive histological observations and morphometric measurements, the present study further summarized tissue lesions using an adapted semi-quantitative grading approach [20–23]. This grading system was introduced to provide a more structured comparison of lesion severity among organs, groups, and sampling time points. Although it was developed with reference to published fish histopathological assessment methods, the present work was originally designed mainly as a descriptive histological and morphometric study; the semi-quantitative grading results should be interpreted as a structured summary of the dominant pathological changes rather than as a fully standardized lesion index system.

5. Conclusions

Short-term exposure to simulated tunnel darkness caused histological alterations in multiple tissues of *S. macropogon*. Gill lamellae exhibited persistent bending and shortening, together with dynamic changes in mitochondria-rich cells. Dorsal muscle fibers showed a reduction in diameter, while intestinal villus height and goblet cell numbers decreased under dark conditions. These results indicate that tunnel darkness can affect the structural stability of the gills, muscle, and intestine of plateau fish. The study provides histological evidence for understanding the physiological effects of tunnel darkness and may contribute to the optimization of lighting conditions in plateau tunnel fishways.

Supplementary Materials: The following are available online at https://www.mdpi.com/article/10.3390/fishes11060340/s1, Table S1: The specific measurements of the fish specimens.

Author Contributions: Conceptualization, T.H., J.L. and Y.W.; Methodology, Y.W. and H.L.; Software, Y.W.; Validation, J.H. and J.Q..; Formal analysis, Y.W. and J.H.; Investigation, Y.W., H.L. and J.H.; Resources, W.L., T.H. and J.L.; Data curation, Y.W. and J.Q..; Writing—original draft preparation, Y.W.; Writing—review and editing, T.H., J.L. and J.Q..; Visualization, Y.W.; Supervision, T.H. and J.L.; Project administration, T.H. and J.L.; Funding acquisition, T.H. and J.L. All authors have read and agreed to the published version of the manuscript.

Funding: This research was supported by Basic Scientific Research Funded Project of Nanjing Hydraulic Research Institute (Y125005) and Natural Science Foundation of Chongqing, China (No. CSTB2025NSCQ-GPX0485).

Institutional Review Board Statement: All animal procedures were approved by the Institutional Animal Care and Use Committee of Southwest University (IACUC-20260317-09; Approval Date: 18 March 2026) and were conducted in accordance with the relevant guidelines and regulations.

Data Availability Statement: The original contributions presented in this study are included in the article/Supplementary Material. Further inquiries can be directed to the corresponding authors.

Acknowledgments: We thank Jiacha Hydropower Plant, Huaneng Tibet Yarlung Zangbo River Hydropower Development & Investment Co., Ltd. (Shannan, Tibet, China) for providing logistical support during the field sampling.

Conflicts of Interest: The author Wei Liu was employed by Jiacha Hydropower Plant, Huaneng Tibet Yarlung Zangbo River Hydropower Development & Investment Co., Ltd. The remaining authors declare that the research was conducted in the absence of any commercial or financial relationships that could be construed as a potential conflict of interest.

References

1. Zhang, J. Ecological and Environmental Impacts of Hydraulic Engineering. *Sci. Technol. Inf.* **2022**, *20*, 130–132.
2. Ma, W.; An, R.; Li, M.; Li, J. Habitat Hydrodynamic Characteristics and Behavior Forecasting for Migratory Fish Downstream of Dams. *J. Beijing Norm. Univ. (Nat. Sci.)* **2021**, *57*, 433–440.
3. Prchalová, M.; Vetesník, L.; Slavík, O. Migrations of Juvenile and Subadult Fish through a Fishpass during Late Summer and Fall. *Folia Zool.* **2006**, *55*, 162–166.
4. Jia, J.; Chen, J.; Long, X. Research Progress of Impact and Countermeasures of Hydropower Development on River Ecological Environment. *J. North China Univ. Water Resour. Electr. Power (Nat. Sci. Ed.)* **2019**, *40*, 62–69.
5. Xu, X.; Liu, D.; Wang, H.; Wang, C. Culvert Fishway Design: Status and Prospects. *J. Yangtze River Sci. Res. Inst.* **2012**, *29*, 44–48.
6. Huang, J.; Lin, C.; Shi, X.; Zhang, N.; Shi, X.; Cheng, B.; Mo, W. Light Environment Optimization of Culvert Fishway Based on the Phototaxis of *Schizothorax prenanti*. *Chin. J. Ecol.* **2021**, *40*, 2155–2163.
7. Tang, H.; Cai, T.; Hu, F. The Fish Phototropic Behavior in Response to Light Characteristics: A Review. *J. Shanghai Ocean. Univ.* **2025**, *34*, 295–306.
8. Xu, J.; Chen, J.; Lin, C.; Liu, Y.; Bai, Y.; Zhang, N.; Yin, R.; Shi, X. The Phototaxis Behavior of *Schizothorax prenanti* in Low Light Intensity. *Chin. J. Ecol.* **2018**, *37*, 2394–2402.
9. Kiessling, A.; Ruohonen, K.; Bjornevik, M. Muscle Fibre Growth and Quality in Fish. *Arch. Fur Tierz.* **2006**, *49*, 137–146.
10. National Forestry and Grassland Administration; Ministry of Agriculture and Rural Affairs. The List of National Key Protected Wild Animals in China. *Chin. J. Wildl.* **2021**, *42*, 605–640.
11. Wei, Y.; Zhang, G.; Huo, B. A Comparative Study on Lactate Dehydrogenase Isozymes in Six Species. *Freshw. Fish.* **2017**, *47*, 3–8.
12. Yang, H.; Huang, D.; Xie, S.; Jian, D.; Chi, S.; Zhang, Q.; Chang, X.; Wang, W.; Fang, Y. Status Quo of Fishery Resources in the Middle Reach of Brahmaputra River. *J. Hydroecology* **2010**, *31*, 120–126.
13. Liu, J. Study on Biology and Population Dynamics of *Schizothorax macropogon* in the Yarlung Tsangpo River. Master's Thesis, Tarim University, Xinjiang, China, 2016.
14. Ma, B.; Wei, K.; Zhao, T.; Pei, F.; Huo, B. Research Progress on the Systematic Evolution and Plateau Adaptation of Schizothoracine Fishes. *J. Lake Sci.* **2023**, *35*, 808–824. [CrossRef]
15. Yang, L.; Wang, Y.; Zhang, Z.; He, S. Comprehensive Transcriptome Analysis Reveals Accelerated Genic Evolution in a Tibet Fish, *Gymnodiptychus pachycheilus*. *Genome Biol. Evol.* **2015**, *7*, 251–261. [CrossRef]
16. Zhou, C.; Zhou, Y.; Xu, L.; Liu, F.; Lei, L.; Gao, H.; Li, J.; Fu, S.; Duan, Y.; Tan, Y.; et al. Chromosome-level Genome Assembly and Population Genomic Analysis Provide Insights into the Genetic Diversity and Adaptation of *Schizopygopsis younghusbandi* on the Tibetan Plateau. *Integr. Zool.* **2024**, *20*, 1246–1264. [CrossRef]
17. Ren, Y.; Nie, Z.; Yang, Z.; Zhang, S.; Wei, J. Morphology and Histology Studies of the Digestive System of *Schizothorax biddulphi*. *Prog. Fish. Sci.* **2020**, *41*, 49–57.
18. Evans, D.H.; Piermarini, P.M.; Choe, K.P. The Multifunctional Fish Gill: Dominant Site of Gas Exchange, Osmoregulation, Acid-Base Regulation, and Excretion of Nitrogenous Waste. *Physiol. Rev.* **2005**, *85*, 97–177. [CrossRef]
19. Liu, J.; Yan, Z.; Yao, B.; Li, Y. Research Progress on the Tissue Structure, Function, Influencing Factors and Protective Substances of Fish Intestine. *Fish. Sci. Technol. Inf.* **2023**, *50*, 121–127.

20. Bernet, D.; Schmidt, H.; Meier, W.; Burkhardt-Holm, P.; Wahli, T. Histopathology in Fish: Proposal for a Protocol to Assess Aquatic Pollution. *J. Fish. Dis.* **1999**, *22*, 25–34. [CrossRef]
21. Saraiva, A.; Costa, J.; Serrão, J.; Cruz, C.; Eiras, J.C. A Histology-Based Fish Health Assessment of Farmed Seabass (*Dicentrarchus labrax* L.). *Aquaculture* **2015**, *448*, 375–381. [CrossRef]
22. Zimmerli, S.; Bernet, D.; Burkhardt-Holm, P.; Schmidt-Posthaus, H.; Vonlanthen, P.; Wahli, T.; Segner, H. Assessment of Fish Health Status in Four Swiss Rivers Showing a Decline of Brown Trout Catches. *Aquat. Sci.* **2007**, *69*, 11–25. [CrossRef]
23. de Jesus, W.B.; Carvalho Neta, R.N.F.; Costa Filho, R.N.D.; Sousa, D.B.P. A Protocol for Assessing Histological Changes and Biometry in *Ucides cordatus* (Crustacea, Decapoda, Ocypodidae) Using Linear Indices. *J. Invertebr. Pathol.* **2025**, *212*, 108386. [CrossRef] [PubMed]
24. Hughes, G.M.; Morgan, M. The Structure of Fish Gills in Relation to Their Respiratory Function. *Biol. Rev.* **1973**, *48*, 419–475. [CrossRef]
25. Alsafy, M.A.M.; Abd-Elhafeez, H.H.; Rashwan, A.M.; Erasha, A.; Ali, S.; El-Gendy, S.A.A. Anatomy, Histology, and Morphology of Fish Gills in Relation to Feeding Habits: A Comparative Review of Marine and Freshwater Species. *BMC Zool.* **2025**, *10*, 3. [CrossRef]
26. Hughes, G.M. Chapter 2—General Anatomy of the Gills. In *Fish Physiology*; Academic Press: Cambridge, MA, USA, 2023; Volume 40, pp. 9–78.
27. Zhao, Q.Y.; Wang, X.D.; Sun, X.J.; Wang, L.L.; Wang, T.Z.; Chen, Q.S.; Lin, J.X. Light and Transmission Electron Microscopic Observation on the Structure of Zebrafish (*Danio rerio*) Gill. *Chin. J. Zool.* **2018**, *53*, 92–98.
28. Elsheikh, E.H. Scanning Electron Microscopic Studies of Gill Arches and Rakers in Relation to Feeding Habits of Some Fresh Water Fishes. *J. Basic Appl. Zool.* **2013**, *66*, 121–130. [CrossRef]
29. Yu, Y.; Liu, J.; Feng, G.; Zhao, F.; Sun, X.; Wang, Y.; Zou, X.; Huang, X.; Li, Q.; Sun, Y.; et al. Effect of Abrupt Salinity Change on Morphology and Structure of Mitochondria-Rich Cells in *Scatophagus argus*. *South China Fish. Sci.* **2021**, *17*, 60–69.
30. Dymowska, A.K.; Hwang, P.P.; Goss, G.G. Structure and Function of Ionocytes in the Freshwater Fish Gill. *Respir. Physiol. Neurobiol.* **2012**, *184*, 282–292. [CrossRef] [PubMed]
31. He, W. Roles of Clock1a in the Zebrafish Circadian Clock. Master's Thesis, Soochow University, Suzhou, China, 2015.
32. Dawson, N.J.; Millet, C.; Selman, C.; Metcalfe, N.B. Measurement of Mitochondrial Respiration in Permeabilized Fish Gills. *J. Exp. Biol.* **2020**, *223*, jeb216762. [CrossRef] [PubMed]
33. Alam, A.N. Structure of Fish Muscles and Composition of Fish. In *Participatory Training of Trainers—A New Approach Applied in Fish Processing*; Bangladesh Fisheries Research Forum: Dhaka, Bangladesh, 2007.
34. Tu, Z.; Yuan, X.; Wang, C.; Xu, X.; Liu, D.; Huang, Y. Swimming Capability and Activity Metabolism of Subadult *Schizothorax macropogon*. *Acta Hydrobiol. Sin.* **2012**, *36*, 682–688. [CrossRef]
35. Rescan, P. Development of Myofibres and Associated Connective Tissues in Fish Axial Muscle: Recent Insights and Future Perspectives. *Differentiation* **2019**, *106*, 35–41. [CrossRef]
36. Li, X. *Aquatic Animal Histology and Embryology*; China Agriculture Press: Beijing, China, 2006.
37. Hvas, M.; Kolarevic, J.; Noble, C.; Oppedal, F.; Stien, L.H. Fasting and its Implications for Fish Welfare in Atlantic Salmon Aquaculture. *Rev. Aquac.* **2024**, *16*, 1308–1332. [CrossRef]
38. Harimana, Y.; Tang, X.; Xu, P.; Xu, G.; Karangwa, E.; Zhang, K.; Sun, Y.; Li, Y.; Ma, S.; Uriho, A.; et al. Effect of Long-Term Moderate Exercise on Muscle Cellularity and Texture, Antioxidant Activities, Tissue Composition, Freshness Indicators and Flavor Characteristics in Largemouth Bass (*Micropterus salmoides*). *Aquaculture* **2019**, *510*, 100–108. [CrossRef]
39. Zhang, Z.; Wang, Q.; Ye, K.; Wang, Z. Effect of Fasting on Body Composition, Muscle Fatty Acid Profiles and Serum Biochemical Parameters of Large Yellow Croaker (*Larimichthys crocea*). *J. Fish. China* **2016**, *40*, 1440–1450.
40. Wang, Y.; Li, X.; Xu, T.; Li, H.; Liu, J.; Yang, Q.; Li, W.; Zidan, S.R.S.; Jiang, C.; Yuan, Y.; et al. Long-Day Photoperiod Improves the Growth and Muscle Quality of Grass Carp (*Ctenopharyngodon idella*). *Foods* **2025**, *14*, 504. [CrossRef] [PubMed]
41. Wu, W.; Ji, H. Overwinter Starvation on Biochemical Composition and Transcriptional Level of Glucose-Lipid-Protein Metabolism Related Genes in Grass Carp (*Ctenopharyngodon idellus*). *Acta Hydrobiol. Sin.* **2022**, *46*, 1618–1630.
42. Peng, L.; Zhang, L.; Xiong, S.; You, J.; Liu, R.; Xu, D.; Huang, Q.; Ma, H.; Yin, T. A Comprehensive Review of the Mechanisms on Fish Stress Affecting Muscle Qualities: Nutrition, Physical Properties, and Flavor. *Compr. Rev. Food Sci. Food Saf.* **2024**, *23*, e13336. [CrossRef]
43. Lavajoo, F.; Perelló-Amorós, M.; Vélez, E.J.; Sánchez-Moya, A.; Balbuena-Pecino, S.; Riera-Heredia, N.; Fernández-Borràs, J.; Blasco, J.; Navarro, I.; Capilla, E.; et al. Regulatory Mechanisms Involved in Muscle and Bone Remodeling during Refeeding in Gilthead Sea Bream. *Sci. Rep.* **2020**, *10*, 184. [CrossRef] [PubMed]
44. Koganti, P.; Yao, J.; Cleveland, B.M. Molecular Mechanisms Regulating Muscle Plasticity in Fish. *Animals* **2020**, *11*, 61. [CrossRef]
45. Wei, J.; Cao, X.; Ren, Y.; Aikebaier, R.; Nie, Z. Anatomy and Histological Observation of Digestive System in *Schizothorax eurystomus*. *South China Fish. Sci.* **2020**, *16*, 120–126.

46. Kumari, P.; Nomani, M.M.R. Study of Intestinal Histopathologies Due to Infestation of *Caryophyllaeus laticeps* (Pallas, 1781) in the Common Carp, *Cyprinus carpio*. *Int. J. Fauna Biol. Stud.* **2022**, *9*, 03–06. [CrossRef]
47. Tang, D. Histological Structure Characteristics and Digestive Enzyme Activities of the Digestive Tract of *Pampus argenteus*. *Acta Hydrobiol. Sin.* **2022**, *46*, 643–653.
48. Firdaus-Nawi, M.; Zamri-Saad, M.; Nik-Haiha, N.Y.; Zuki, A.B.; Effendy, A.W.M. Histological Assessments of Intestinal Immuno-Morphology of Tiger Grouper Juvenile, *Epinephelus fuscoguttatus*. *SpringerPlus* **2013**, *2*, 611. [CrossRef] [PubMed]
49. Wilson, J.M.; Castro, L.F.C. Morphological Diversity of the Gastrointestinal Tract in Fishes. *Fish. Physiol.* **2010**, *30*, 1–55.
50. Salinas, I. The Mucosal Immune System of Teleost Fish. *Biology* **2015**, *4*, 525–539. [CrossRef]
51. Gonçalves, M.; Lopes, C.; Silva, P. Comparative Histological Description of the Intestine in Platyfish (*Xiphophorus maculatus*) and Swordtail Fish (*Xiphophorus Helleri*). *Tissue Cell* **2024**, *87*, 102306. [CrossRef]
52. Gong, Y. The Observation on Morphology and Histology of Digestive Tract in *Ophicephalus argus*. *Open J. Fish. Res.* **2017**, *4*, 79–84. [CrossRef]
53. Zhang, S.; Liang, Y.; Sun, X.; Su, J.; Jiang, Z.; Guo, Z.; Ma, J. Effects of Starvation and Subsequent Feeding on Morphological and Histological Structure of Digestive System in *Platichthys stellatus*. *J. Fish. Sci. China* **2013**, *19*, 445–452. [CrossRef]
54. Qian, Z.; Xu, J.; Liu, H.; Cui, M.; Zhang, C. Effects of Flow Velocity on Growth Performance and Physiological and Biochemical Indexes of Large Yellow Croaker (*Larimichthys crocea*) in Welfare Aquaculture. *South China Fish. Sci.* **2025**, *21*, 53–63.
55. Loureiro Paschoalini, A.; Boaventura, T.P.; Costa dos Santos, F.A.; Bazzoli, N.; Luz, R.K.; Favero, G.C. Morphological and Histochemical Changes in the Intestine of Adult Catfish (*Lophiosilurus alexandri*) Subjected to Chronic Fasting and Refeeding. *J. Appl. Aquac.* **2025**, *37*, 193–207. [CrossRef]

Disclaimer/Publisher's Note: The statements, opinions and data contained in all publications are solely those of the individual author(s) and contributor(s) and not of MDPI and/or the editor(s). MDPI and/or the editor(s) disclaim responsibility for any injury to people or property resulting from any ideas, methods, instructions or products referred to in the content.